Structural analysis of the Cu(100)-$p(2 \times 2)$-Sn surface using low and medium energy ion scattering spectroscopies

M. Walker,[*] M. G. Brown, M. Draxler,[†] M. G. Dowsett, and C. F. McConville[‡]
Department of Physics, University of Warwick, Coventry, CV4 7AL, United Kingdom

T. C. Q. Noakes and P. Bailey
STFC Daresbury Laboratory, Daresbury, Warrington, WA4 4AD, United Kingdom
(Received 29 October 2010; published 25 February 2011)

The atomic structure of the Cu(100)-$p(2 \times 2)$-Sn surface has been studied using medium energy ion scattering (MEIS), co-axial impact collision ion scattering spectroscopy (CAICISS), low energy electron diffraction (LEED), and Auger electron spectroscopy (AES). The complex $p(2 \times 2)$-based LEED pattern with antiphase domains was observed at an estimated Sn coverage of 0.21 ML, confirmed with AES. The existence of subsurface Sn atoms was immediately ruled out by the lack of blocking dips in the MEIS Sn scattered yield, whereas the initial analysis of the CAICISS data ruled out the three overlayer models, allowing quantitative fitting to focus on the Cu-Sn substitutional surface alloy model. The fitted model showed that the surface relaxed outward following Sn deposition and also demonstrated an out-of-plane shift of Sn atoms in the outermost layer.

DOI: 10.1103/PhysRevB.83.085424 PACS number(s): 61.05.Np, 61.05.jh, 68.35.bd

I. INTRODUCTION

Metal-on-metal epitaxial growth affords the opportunity to control the structural, chemical, and electronic behavior of bimetallic surfaces, leading to differing characteristics when compared to the surfaces of fully alloyed materials.[1,2] The interaction of metallic adsorbates with the surface of Cu crystals has been widely investigated due to potential applications in metallic thin film growth[3–6] and catalytic processes.[7,8] In some cases the formation of bimetallic surfaces can lead to complex surface structures,[9–14] with the deposition of submonolayer coverage of Sn on to the clean Cu(100) surface being a particularly interesting example due to the large mismatch in atomic radii (∼10 %) between Cu and Sn.[15] This particular system exhibits five different reconstructions in the submonolayer range,[16–21] summarized in Table I.

The Phase I structure, based on a Cu(100)-$p(2 \times 2)$-Sn superstructure was first reported by Argile and Rhead,[16] who observed a "complex" pattern which indicated the presence of antiphase domains. McLoughlin's low energy electron diffraction (LEED) I-V studies[17] of this system at a Sn coverage of 0.21 ML reinforced the notion of a $p(2 \times 2)$-based superstructure and proposed models based on the optimal coverage of 0.25 ML which incorporated "light" domain walls. Similar domain walls have been observed in the Cu(100)/Pb,[22] Rh(100)/La,[23] and Cu(100)/Bi[24] systems. The results of subsequent scanning tunneling microscopy (STM) and normal incidence x-ray standing wave (NIXSW) studies by Cafolla[25] supported the domain wall model, proposing three potential adsorption sites: fourfold hollow site, substitutional alloy site, or atop site. Three widths of domain wall were also proposed, containing one, three, and five Cu rows. While the STM and NIXSW analysis favored the substitutional alloy model, the evidence was not conclusive. In order to resolve this problem, we have employed both low and medium energy ion scattering spectroscopic techniques, with the experimental conditions arranged so that the surface layer can be examined in a highly accurate manner. In addition to the three Sn adsorption sites proposed by Cafolla,[25] we also examine Sn atoms located in bridge sites above the outermost Cu layer. All four models are shown in Fig. 1.

The main focus of this article is to resolve the Phase I structure of the Cu(100)-Sn system, but it also provides a clear demonstration of the ability to combine low and medium energy ion scattering techniques to resolve pressing problems within modern science. Such techniques can be utilized to resolve the reconstructed surface structures of semiconductors, as well as other complex catalytic surfaces. As device dimensions decrease, the structural properties of surfaces and interfaces become ever more important, with ion scattering techniques ideally placed to play an important role in their characterization.

II. EXPERIMENTAL AND ANALYSIS DETAILS

In this paper we examine the Cu(100)-$p(2 \times 2)$-Sn structure using both coaxial impact collision ion scattering spectroscopy (CAICISS) at the University of Warwick[26,27] and the medium energy ion scattering (MEIS) facility at Daresbury Laboratory.[28,29] Both chambers were equipped with Auger electron spectroscopy (AES) and LEED for the analysis of surface cleanliness and reconstruction, respectively. In both chambers cleaning of the Cu(100) surface was achieved using multiple cycles of ion bombardment with Ar^+ ions at 1.5 keV for 20 min, followed by annealing at 750 °C for 60 min,[30] until the AES spectrum showed no signs of surface contamination and a sharp (1×1) LEED pattern with low background intensity was observed.

Controlled deposition of Sn (5N purity) was carried out using a water-cooled Knudsen cell evaporator (W. A. Technology), held at a steady temperature of 950 °C. This temperature provided a constant deposition rate of 0.012 ± 0.002 ML min^{-1}, calculated using the established coverages of observed LEED patterns which are detailed in Table I. In

TABLE I. Summary of the reconstructions reported following Sn deposition on to the clean Cu(100) surface at submonolayer coverage.[16–21] The Phase I structure is the subject of this investigation.

Phase	Sn coverage (ML)	Reconstruction
I	0.21	$p(2 \times 2)$
II	0.33	$p(2 \times 6)$
II S (2.5)	0.38	Complex $c(4 \times 8)$
III	0.50	$p(3\sqrt{2} \times \sqrt{2})R45^{\circ}$
IV	0.625	$c(4 \times 4)$

both chambers, the pressure remained below 5×10^{-10} mbar throughout the Sn deposition process. Sn was deposited for 18 min in order to establish the optimal Phase I LEED pattern. Using the calibration rate above, the surface Sn coverage was estimated to be 0.216 ± 0.036 ML, very close to the coverage reported in the study of McLoughlin.[17]

A. Medium energy ion scattering MEIS

The duoplasmatron ion source[29] produced a beam of H^+ ions with a nominal primary energy of 100 keV, incident on the Cu(100) surface with a beam spot size of approximately 0.5×1.0 mm. The end station comprises four separate ultrahigh vacuum chambers: the scattering chamber, a fast entry chamber for sample introduction, a sample storage chamber, and a preparation chamber equipped with LEED, AES, sample cleaning facilities, and deposition sources. Sample transfer between the chambers was achieved under ultrahigh vacuum conditions, with the scattering, storage, and preparation chambers all possessing base pressures of 1×10^{-10} mbar. Two different room temperature MEIS experiments were conducted, with the sample aligned on a high precision goniometer such that the incident H^+ beam was directed along either the $\langle 011 \rangle$ or $\langle 112 \rangle$ azimuths within the Cu(100) structure. Figure 2 shows that the chosen incident directions illuminate one and two atomic layers, respectively, demonstrating the highly surface specific nature of MEIS double-alignment experiments.[31] Figure 2 and Table II detail the different crystallographic directions in which the scattered ions are blocked, leading to a variation of detected intensity with scattering angle.

Incident ion doses were limited to ~ 20 μC per data set, corresponding to $\sim 10^{16}$ ions per cm^2, with the beam moved to a new position on the sample prior to the next set of data being recorded. Ions scattered from the surface were detected using a toroidal electrostatic analyzer (TEA),[32] which provides "tiles" of scattered ion yield as a function of both scattering angle and energy. Each tile contains 27° of angular data and encompasses an energy range that is a fixed percentage of the pass energy at the top of each tile. By recording multiple tiles in different energy ranges (see Fig. 3), or different detector orientations, one can build up a picture of the atomic structure and composition of the surface via the creation of energy or angular intensity maps, commonly referred to as energy spectra and blocking curves, respectively. In this investigation, data were collected in three adjacent detector positions per incident geometry in order to generate blocking curves over a range of scattering angles approaching 60°. Three sets of data were recorded in each incident direction to improve the statistics of the experiment. Analysis of the blocking curves using the XVEGAS code[33,34] leads to the determination of the atomic structure and elemental composition of the outermost few atomic layers. XVEGAS employs the Thomas-Fermi-Molière potential,[35] with thermal vibrations calculated using a Monte Carlo algorithm. This approach has been successfully applied to many metal-based surface structure determinations in recent years.[29,36–39]

B. Coaxial impact collision ion scattering spectroscopy

CAICISS is a novel low energy ion scattering technique, with the only UK-based system located at the University of

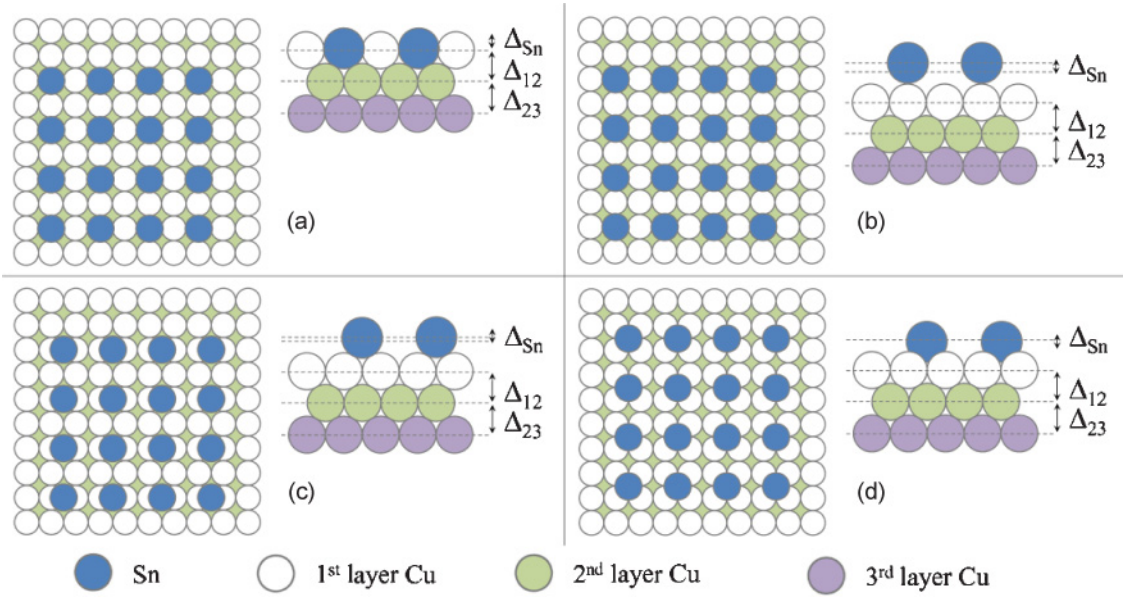

FIG. 1. (Color online) The four models of the Cu(100)-$p(2 \times 2)$-Sn (Phase I) surface examined in this study: (a) substitutional alloy; (b) atop overlayer; (c) bridge site overlayer; (d) fourfold hollow site overlayer.

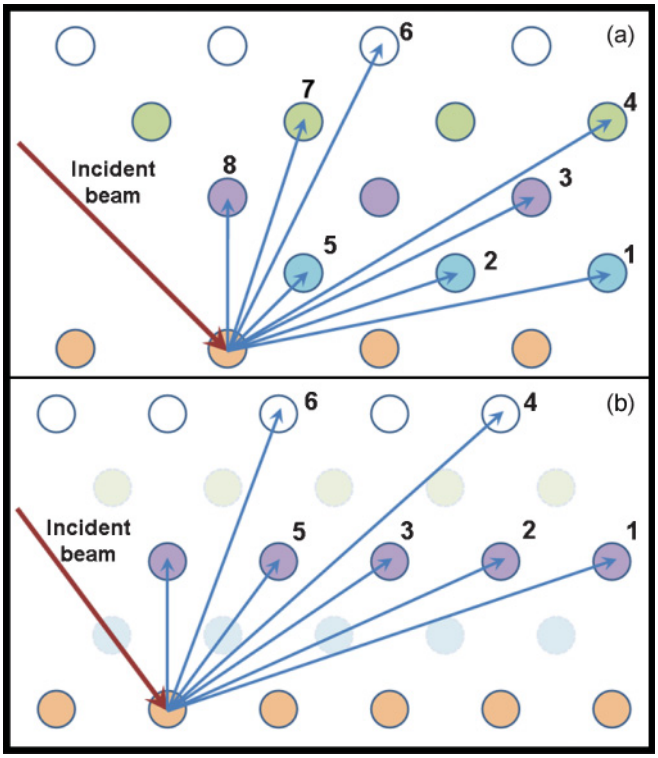

FIG. 2. (Color online) A schematic of the scattering geometries in (a) the ⟨011⟩ and (b) the ⟨112⟩ incident directions. The paler atoms shown in the ⟨112⟩ geometry are out-of-plane with respect to the emboldened atoms. In the ⟨011⟩ direction, only the outermost layer is "illuminated" by the beam, focusing the incident flux on to the subsurface layers. Two layers are illuminated in the ⟨112⟩ geometry (i.e., one layer on both the emboldened and paler colored planes). Scattering angles and the corresponding crystallographic directions are given in Table II.

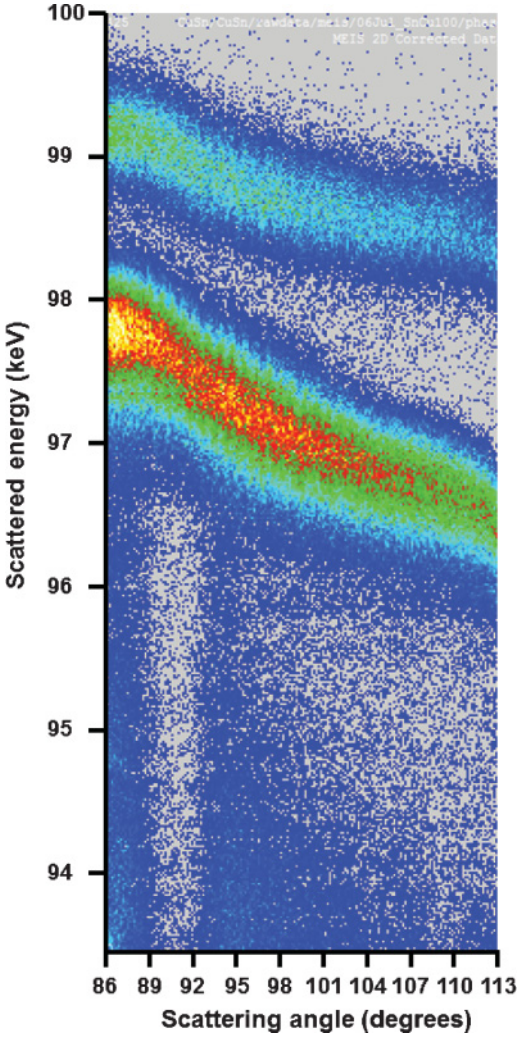

FIG. 3. (Color online) MEIS scattered intensity (color scale) as a function of scattered energy and scattering angle recorded from the Phase I surface using 100 keV He^+ ions incident in the ⟨112⟩ azimuth. The upper signal (∼99 keV) corresponds to scattering from Sn atoms at the surface. The lower signal (∼97 keV) corresponds to scattering from Cu atoms near the surface. The bulk blocking along the ⟨111⟩ direction can be seen at 90°.

Warwick. Ions and neutrals which are scattered through angles between 178° and 179.8° are detected in time-of-flight (ToF) mode in order to derive the elemental composition, while the detected intensity variation with angular rotation of the sample leads to the determination of the atomic structure.[27,35] Due to its inherent surface specificity,[35] the technique is ideally suited to the study of complex bimetallic surfaces whose constituents have a significant mass difference (almost 1:2 in the case of the Cu/Sn system). The makeup of the system and its operation are described elsewhere.[26,27]

TABLE II. Summary of the scattering geometries relevant to the MEIS spectra recorded during the study of the Cu(100)-$p(2 \times 2)$-Sn surface. Note θ represents the total scattering angle. See Fig. 2 for an illustration.

⟨011⟩ Incidence			⟨112⟩ Incidence		
No.	θ (degrees)	⟨hkl⟩	No.	θ (degrees)	⟨hkl⟩
1	56.31	⟨05$\bar{1}$⟩	1	74.21	⟨22$\bar{1}$⟩
2	63.43	⟨03$\bar{1}$⟩	2	79.96	⟨33$\bar{2}$⟩
3	71.57	⟨02$\bar{1}$⟩	3	90.00	⟨11$\bar{1}$⟩
4	75.96	⟨05$\bar{3}$⟩	4	98.05	⟨33$\bar{4}$⟩
5	90.00	⟨01$\bar{1}$⟩	5	109.48	⟨11$\bar{2}$⟩
6	108.43	⟨01$\bar{2}$⟩	6	125.27	⟨11$\bar{4}$⟩
7	116.56	⟨01$\bar{3}$⟩	7	144.74	⟨00$\bar{1}$⟩
8	135.00	⟨00$\bar{1}$⟩			

In the experiments detailed below, a primary beam of 3.0 keV He^+ ions was directed onto the sample along the ⟨100⟩ and ⟨110⟩ azimuths. These directions were chosen as they should yield the most obvious differences in both Cu and Sn backscattered intensities between the three overlayer models and the alloy model. The main scattering geometries which generate peaks in the CAICISS polar angle scans from the Cu(100) surface in the ⟨110⟩ direction via trajectory focusing[35] are shown in Fig. 4, showing how a CAICISS polar angle scan allows one to probe the outermost few atomic layers. Backscattered intensity data were collected as a function of ToF in 1.8° polar angle steps. The individual polar angle plots were then collated in order to produce a three-dimensional plot of intensity versus ToF and polar angle.

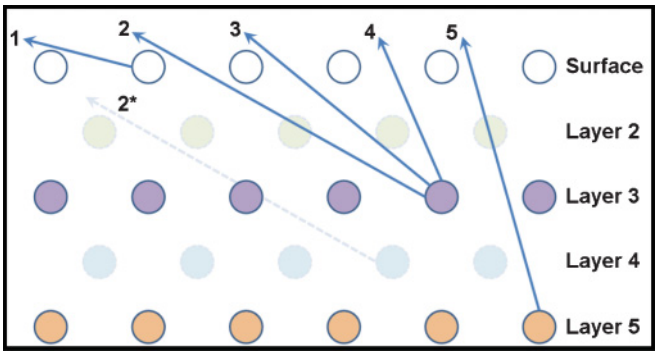

FIG. 4. (Color online) A schematic of the scattering geometries that generate peaks in the CAICISS polar angle scans in the ⟨110⟩ azimuth. The atoms in the even-numbered layers lie out-of-plane with respect to the atoms in the odd-numbered layers, generating additional contributions to peak intensities (e.g., 2 and 2*).

The ToF ranges corresponding to elastic scattering from each constituent element of the surface region, in this case Sn and Cu, were calculated and the intensities from all of the polar angle plots integrated over these time ranges in order to produce a backscattered intensity plot as a function of polar angle for each element.[27] The plots were analyzed using the FAN code developed by Niehus and Spitzl,[40] in conjunction with an implicit filtering for constrained optimization (IFFCO) fitting routine, detailed later, in order to accurately establish the atomic structure and composition of the Phase I surface. FAN simulations were performed using a 60% enhancement to the surface vibration amplitudes.[41] Through a previous investigation,[42] we have established that a reduced screening length correction must be used in the Molière approximation within the Thomas-Fermi (TFM) interaction potential for analysis of CAICISS polar angle spectra. In the analysis of this experiment we have employed correction factors of 0.58 and 0.70 for Cu and Sn, respectively.

C. Structural optimization using IFFCO

IFFCO is an algorithm for optimizing functions with multiple minima which has been applied to many different problems in modern science.[43–49] The algorithm optimizes functions using a decreasing sequence of finite difference steps to approximate the gradient. We have applied this method in the analysis of MEIS and CAICISS experiments through combination with ion scattering simulation codes. In the IFFCO optimization, an initial value for one of the simulation input parameters (such as an interlayer spacing, elemental composition, or screening correction factor) is chosen, a FAN or XVEGAS simulation performed and an *R*-factor calculated by comparing the simulation output to the experimental data. The chosen parameter is then changed and the process repeated until a *R*-factor curve for the parameter has been produced. This defines the range of values for each parameter used during the final parallel optimization of all parameters in order to obtain a final structural and compositional fit. In this analysis we have used the χ^2 *R*-factor which has been successfully applied in many MEIS studies.[29,36–39]

III. RESULTS AND DISCUSSION

A. LEED and AES

Following cleaning, the Cu(100) surface exhibited a sharp (1 × 1) LEED pattern at 74 eV, shown in Fig. 5(a). Subsequently, Sn was deposited on to the surface for 18 min, after which a $p(2 \times 2)$ pattern was observed at 91 eV, shown in Fig. 5(b). Figure 5(c) presents a sketch of the pattern from the paper by Argile and Rhead,[16] showing that the Phase I surface had been formed.

AES data were recorded using a primary electron beam energy of 5 keV, at which the relative sensitivity of the Sn MNN transition is approximately 3.5 times higher than that of the Cu LMM transition.[50] The Auger results, not shown here, exhibited no signs of contamination as a result of the deposition process. The Cu LMM transitions were observed at kinetic energies between 740 and 940 eV, with the Sn MNN transitions being observed between 325 and 450 eV. Importantly there was no evidence of O (510 eV) or C (272 eV) in the spectrum. These LEED and AES results allow us to be confident that the application of MEIS and CAICISS to this system will enable an accurate surface structure determination of a well-ordered Phase I surface, free from any effects due to surface contamination.

B. Ion scattering: preliminary analysis

1. Sn penetration into the Cu(100) structure

The first step in the ion scattering data analysis was to determine whether the deposited Sn atoms had penetrated below the surface of the Cu(100) structure. If Sn atoms are

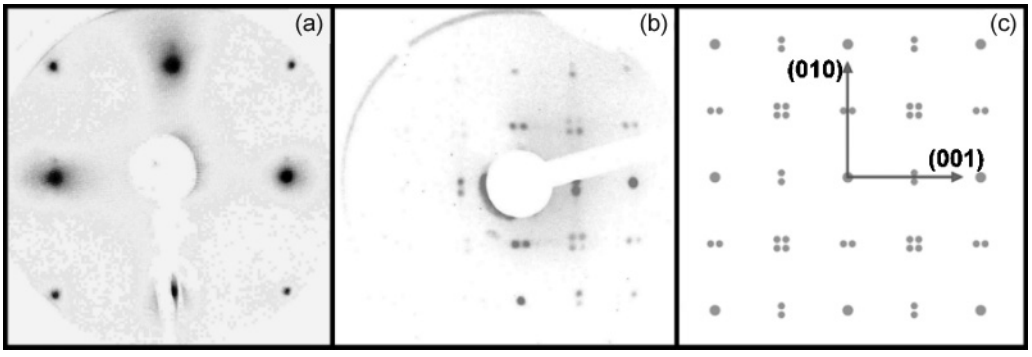

FIG. 5. LEED observations during the preparation of the Phase I Cu(100)-$p(2 \times 2)$-Sn surface. (a) The Cu(100)-(1 × 1) surface at 74 eV; (b) the Cu(100)-$p(2 \times 2)$-Sn surface at 91 eV; (c) a schematic of the Phase I LEED pattern from Argile and Rhead.[16]

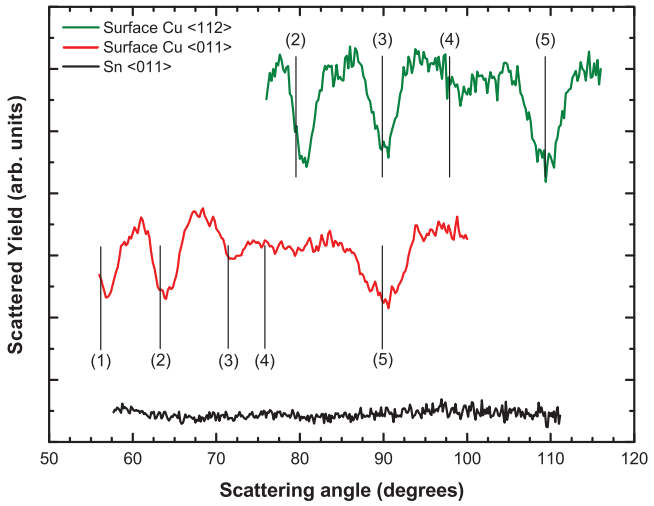

FIG. 6. (Color online) MEIS blocking curves for the surface Cu signal in both the ⟨112⟩ (upper curve) and ⟨011⟩ (middle curve) incident directions. Each of the blocking dips are labeled corresponding to the information given in Table II. The surface Sn signal from the ⟨011⟩ incidence geometry is also shown (lower curve), exhibiting no blocking dips and hence illustrating that all of the adsorbed Sn resides in the outermost layer.

located below the surface then blocking dips should be present within the MEIS Sn scattered yield due to blocking from atoms along the exit trajectory. Figure 3 shows the plot of MEIS scattered intensity (color scale) versus both scattered energy and scattering angle. By projecting these data onto the angular axis, the blocking curves for both Cu and Sn atoms at the surface were extracted (see Fig. 6). The Sn scattered intensity curve clearly shows a complete absence of blocking dips in the ⟨011⟩ incident geometry. A similar signal was extracted from the ⟨112⟩ incidence data (not shown). Also shown are the blocking curves arising from ions scattered from Cu atoms in the surface region in both the ⟨011⟩ and ⟨112⟩ incidence directions, with the blocking dips numbered in such a way as to correspond with the directions shown in Fig. 2. This provides conclusive evidence that the deposited Sn atoms remain on the surface of the Cu(100) structure with no detectable penetration below the surface. Therefore subsequent analysis of all ion scattering data focused on the four models proposed in Fig. 1, using the Cu signal to fit the data.

2. *Assessing the models with MEIS*

Initial XVEGAS simulations of the MEIS blocking curves from the four models are shown in comparison to the experimental data in Figs. 7 and 8. Both angular and intensity discrepancies exist for all of the models, as one would expect given the use of bulk interlayer spacings in these initial simulations. In the ⟨011⟩ direction the only major difference between the simulated curves is an extra blocking dip in the atop model at 78°. There are indications at around scattering angles of 100° in the ⟨112⟩ direction that the alloy and hollow site models offer a more accurate reproduction of the experimental data. In addition, the atop model fails to reproduce the blocking intensity at 80° and 110°. However, this evidence is not conclusive enough to rule out any of the four models at this stage.

3. *Assessing the models with CAICISS*

CAICISS data were recorded using a beam of 3.0 keV He^+ ions, incident in the ⟨100⟩ and ⟨110⟩ azimuths. The

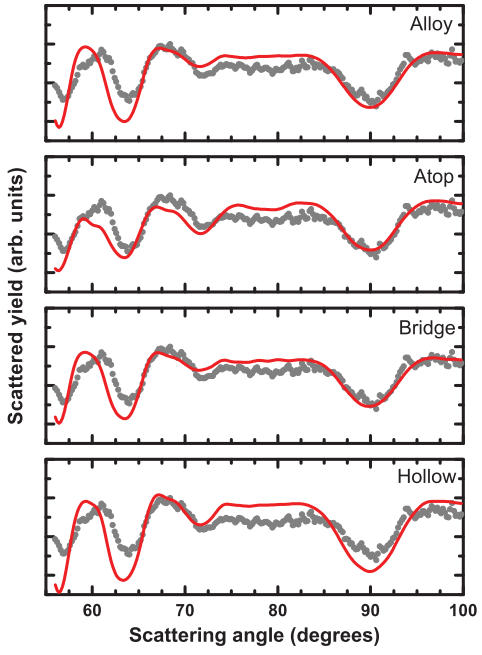

FIG. 7. (Color online) The comparison of Cu surface peak blocking curves with XVEGAS simulations in the ⟨011⟩ incidence geometry. The experimental data are represented by the gray points; the simulations are in red.

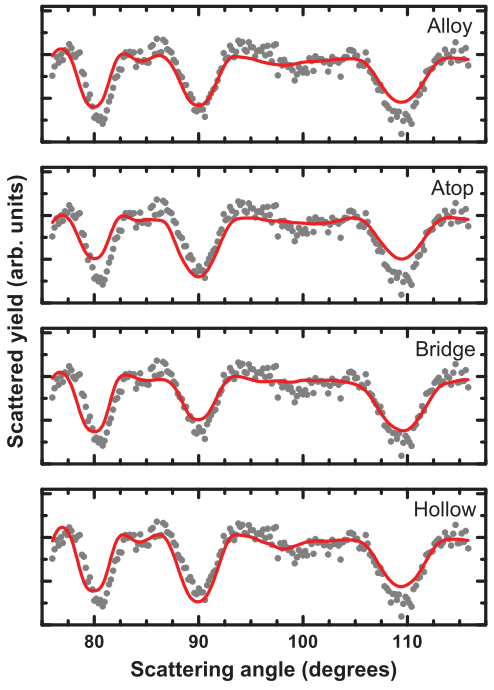

FIG. 8. (Color online) The comparison of Cu surface peak blocking curves with XVEGAS simulations in the ⟨112⟩ incidence geometry. The experimental data is represented by the gray points; the simulations are in red.

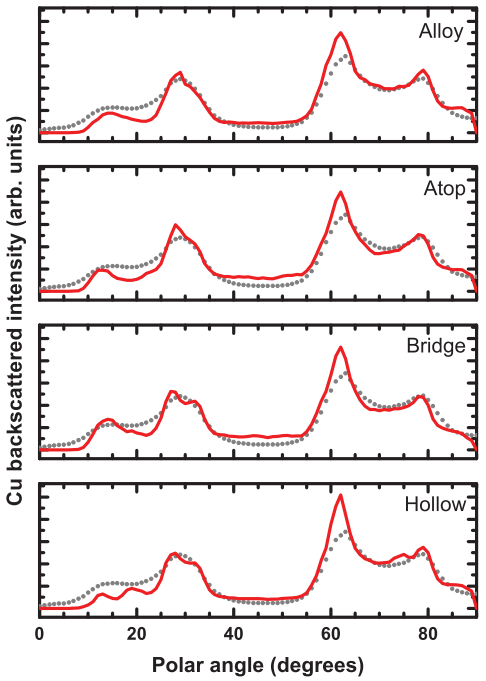

FIG. 9. (Color online) CAICISS experimental data recorded in the ⟨100⟩ azimuth (gray dots) and FAN simulations (solid red lines) of the four Cu(100)-$p(2 \times 2)$-Sn trial structures.

symmetry of the structure about the surface normal in these directions means that collecting data over a 0° to 90° polar angle range is sufficient to describe the atomic structure. The Cu-backscattered profiles extracted from the experimental data recorded in the ⟨100⟩ and ⟨110⟩ incident azimuths are shown in Figs. 9 and 10, respectively. Also shown are FAN simulations of each of the four models using bulk Cu(100) interlayer spacings.

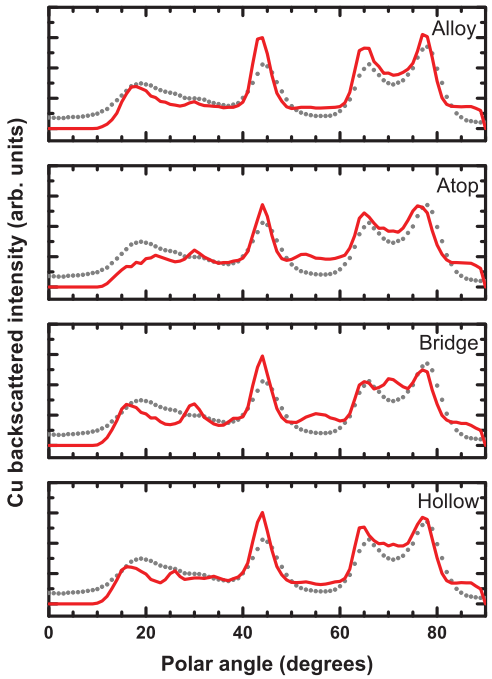

FIG. 10. (Color online) CAICISS experimental data recorded in the ⟨110⟩ azimuth (gray dots) and FAN simulations (solid red lines) of the four Cu(100)-$p(2 \times 2)$-Sn trial structures.

TABLE III. *R*-factors produced by IFFCO following the initial simulation of CAICISS data for each of the four proposed models. The values shown are an average of the values calculated in the ⟨100⟩ and ⟨110⟩ incidence directions.

Model	CAICISS *R*-factor
Surface alloy	4.9
Overlayer (atop)	7.9
Overlayer (bridge)	6.6
Overlayer (hollow)	5.5

Analysis of the data recorded in the ⟨100⟩ direction reveals little difference between the models, with only the fourfold hollow site model being ruled out due to the shape of the profile at polar angles less than 25°.

Analysis of the experimental data recorded in the ⟨110⟩ azimuth reveals a clear difference between the four models. Here, only the substitutional alloy provides an accurate replication of the surface peak (19° in the experimental data), with significant angular and intensity discrepancies existing for all the other models. In addition, the three overlayer models give rise to an additional peak at 70°, which does not exist in the experimental data. Hence the CAICISS data recorded in the ⟨110⟩ azimuth provides conclusive evidence that the substitutional alloy model is the most appropriate model to pursue in the optimized fitting of both MEIS and CAICISS data. This choice is reinforced by the *R*-factors produced by IFFCO for each of the models (shown in Table III).

C. Optimized fitting of the alloy model

1. MEIS

XVEGAS simulations in conjunction with the IFFCO optimization routine were conducted for the surface alloy model in both the ⟨011⟩ and ⟨112⟩ directions, the final results of which are shown in Fig. 11. Three structural parameters were fitted, Δ_{Sn}, Δ_{12}, and Δ_{23}, as shown in Fig. 1(a). The analysis reveals an out-of-plane shift of Sn atoms of 0.10 ± 0.18 Å

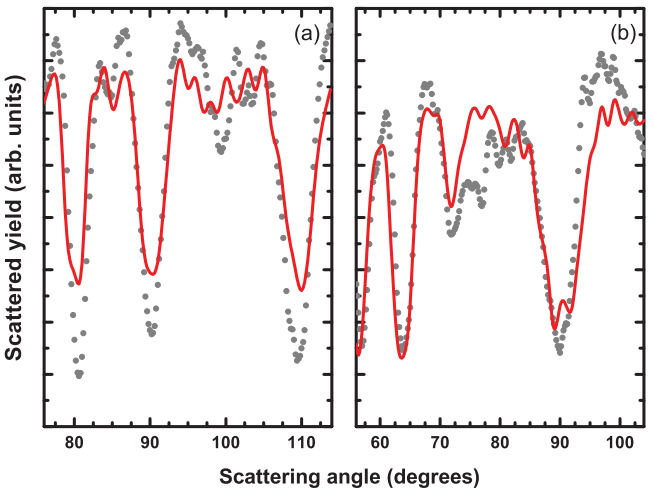

FIG. 11. (Color online) The final fits produced by the IFFCO optimization of XVEGAS simulations (solid red curve), relative to the experimental MEIS data (gray dots); (a) ⟨011⟩ incidence and (b) ⟨112⟩ incidence.

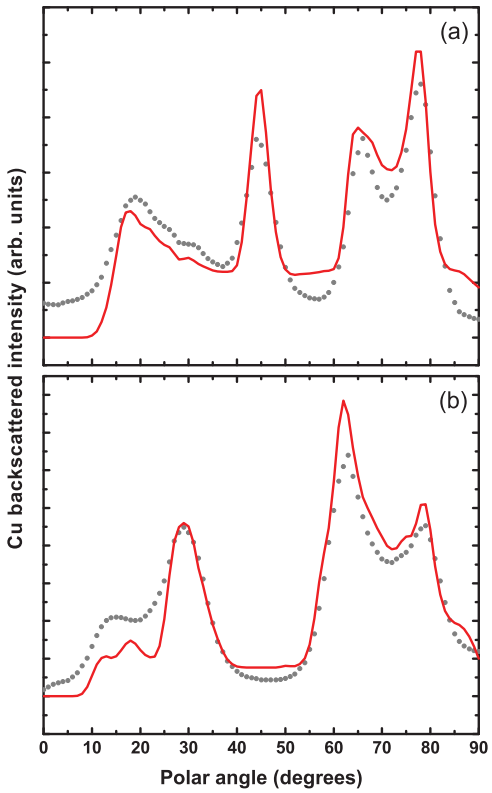

FIG. 12. (Color online) The final fits produced by the IFFCO optimization of FAN simulations (solid red curve), relative to the experimental CAICISS data (gray dots); (a) ⟨110⟩ incidence and (b) ⟨100⟩ incidence.

and an expansion of Δ_{12} of 0.03 ± 0.03 Å over the bulk Cu(100) interlayer spacing of 1.808 Å. The change in Δ_{12} actually represents an outward relaxation of 0.09 Å (5%) over the first interlayer spacing on the clean Cu(100) surface.[27] Such outward relaxations are to be expected as a mechanism of surface strain relief given the difference in atomic radii between Sn and Cu. The final model returned a combined *R*-factor from the two simulated directions of 4.0, down from the value of 11.5 produced using bulklike interlayer spacings.

2. *CAICISS*

FAN simulations in conjunction with IFFCO optimization were also employed to quantitatively analyze the CAICISS data recorded in the ⟨100⟩ and ⟨110⟩ incident azimuths, the results of which are shown in Fig. 12. A good fit of the data was realized in both azimuths, with the final structure including an out-of-plane shift of Sn atoms of 0.01 ± 0.16 Å and an expansion of Δ_{12} of 0.03 ± 0.01 Å over the bulk Cu(100) interlayer spacing of 1.808 Å. Both of these values agree within experimental error with the values derived from the MEIS data. The final model returned a combined *R*-factor from the two simulated directions of 4.4, down from the value of 4.9 produced using bulklike interlayer spacings.

Finally, we turn our attention to the composition of the domain walls separating the 4 × 4 unit cell areas in which the (2 × 2) structure is found [see Fig. 1(a)]. Using STM, Cafolla *et al.*[25] reported domain walls comprising one, three, and five rows of Cu atoms. The combination of techniques used here only facilitates the determination of the domain wall structure averaged over an area of approximately 1.5 mm^2. Analysis of the Cu backscattered intensity at low polar angles (i.e., the surface peak) provides an insight into how much Cu is on the surface. Altering the width of the domain walls significantly changes the amount of Cu on the surface in the simulations, hence impacting on the surface peak intensity. Similarly, knowing the deposition rate of the Knudsen cell, one can estimate how much Sn has been deposited onto the surface. Bearing all this in mind, the Cu-Sn surface alloy model best replicates the experimental CAICISS data, with domain walls comprising two rows of Cu atoms, suggesting that the majority of domain walls are either one or three rows wide. An average domain wall width of two rows leads to an Sn coverage of 0.20 ML, corresponding well with the 0.21 ML coverage estimated from the deposition rate of the Knudsen cell.

TABLE IV. Structural parameters for the Cu(100)-$p(2 \times 2)$-Sn surface alloy deduced from analysis of the MEIS and CAICISS data presented in this report. See Fig. 1(a) for an illustration of these parameters.

Parameter	MEIS	CAICISS
Δ_{Sn} (Å)	0.10 ± 0.18	0.01 ± 0.16
Δ_{12} (Å)	0.03 ± 0.03	0.03 ± 0.01
Δ_{23} (Å)	0.01 ± 0.04	0.10 ± 0.01
R-factor	4.0	4.4

IV. SUMMARY

In this article we have reported a surface structural study on the Cu(100)-$p(2 \times 2)$-Sn surface, Phase I of the submonolayer reconstructions of the Cu(100)/Sn system. Using preliminary MEIS analysis it was determined that all of the Sn atoms reside in the outermost layer via the lack of blocking dips in the Sn scattered yield. XVEGAS simulations indicated that the atop site overlayer and bridge site overlayer models did not fit the experimental data. More conclusive evidence came from the CAICISS data recorded in the ⟨110⟩ incident azimuth, showing erroneous polar angle spectra from the fourfold hollow, atop, and bridge site overlayers. The substitutional alloy was the only model to accurately reproduce the polar angle spectrum and hence it was selected for optimized fitting using the IFFCO routine. The combined fitting of both MEIS and CAICISS data revealed an out-of-plane shift for the Sn atoms relative to the Cu atoms in the surface layer, in conjunction with an outward relaxation of the surface layer with respect to the bulk Cu(100) structure (summarized in Table IV).

ACKNOWLEDGMENTS

We thank Rob Johnston for technical support during this investigation, and STFC Daresbury Laboratory for access to the MEIS facility and support during the experiments. The authors acknowledge support from the Engineering and Physical Sciences Research Council (EPSRC) under Grant No. EP/E003370/1. M.G.B. acknowledges the EPSRC for funding from the Doctoral Training Account.

*m.walker@warwick.ac.uk
†Current address: High Tech Coatings GmbH, Dr.-Mitterbauer-Strasse 3, A-4655 Vorchdorf, Austria.
‡c.f.mcconville@warwick.ac.uk

[1]U. Bardi, Rep. Prog. Phys. **57**, 939 (1994).
[2]J. A. Rodriguez, Surf. Sci. Rep. **24**, 223 (1996).
[3]F. Abel, C. Cohen, J. A. Davies, J. Moulin, and D. Schmaus, Appl. Surf. Sci. **44**, 17 (1990).
[4]M. T. Kief and W. F. Egelhoff Jr., Phys. Rev. B **47**, 10785 (1993).
[5]E. AlShamaileh, H. Younis, C. J. Barnes, K. Pussi, and M. Lindroos, Surf. Sci. **515**, 94 (2002).
[6]M. Walker, C. R. Parkinson, M. Draxler, and C. F. McConville, Surf. Sci. **584**, 153 (2005).
[7]I. Nakamura, H. Nakano, T. Fujitani, T. Uchijima, and J. Nakamura, Surf. Sci. **402-404**, 92 (1998).
[8]J. M. Campbell, J. Nakamura, and C. T. Campbell, J. Catal. **136**, 24 (1992).
[9]P. T. Sprunger, E. Lægsgaard, and F. Besenbacher, Phys. Rev. B **54**, 8163 (1996).
[10]T. Aruga, Surf. Sci. Rep. **61**, 283 (2006).
[11]M. Batzill, D. Beck, and B. E. Koel, Surf. Sci. **558**, 35 (2004).
[12]C. T. Campbell, Annu. Rev. Phys. Chem. **41**, 775 (1990).
[13]Y. Gauthier, W. Moritz, and W. Hösler, Surf. Sci. **345**, 53 (1996).
[14]T. Nakagawa, S. Mitsushima, H. Okuyama, M. Nishijima, and T. Aruga, Phys. Rev. B **66**, 085402 (2002).
[15]J. C. Slater, J. Chem. Phys **41**, 3199 (1964).
[16]C. Argile and G. E. Rhead, Thin Solid Films **87**, 265 (1982).
[17]E. McLoughlin, A. A. Cafolla, E. AlShamaileh, and C. J. Barnes, Surf. Sci. **482-485**, 1431 (2001).
[18]K. Pussi, E. AlShamaileh, E. McLoughlin, A. A. Cafolla, and M. Lindroos, Surf. Sci. **549**, 24 (2004).
[19]J. Lallo, L. V. Goncharova, B. J. Hinch, S. Rangan, R. A. Bartynski, and D. R. Strongin, Surf. Sci. **602**, 2348 (2008).
[20]Y. Nara, K. Yaji, T. Iimori, K. Nakatsuji, and F. Komori, Surf. Sci. **601**, 5170 (2007).
[21]J. Martínez-Blanco, V. Joco, P. Segovia, T. Balasubramanian, and E. G. Michel, Appl. Surf. Sci. **252**, 5331 (2006).
[22]F. Bocquet and S. Gauthier, Surf. Sci. **416**, 1 (1998).
[23]M. Kildemo, T. Ramsvik, and S. Raaen, Surf. Sci. **490**, 1 (2001).
[24]H. L. Meyerheim, M. D. Santis, W. Moritz, and I. K. Robinson, Surf. Sci. **418**, 295 (1998).
[25]A. A. Cafolla, E. McLoughlin, E. AlShamaileh, P. Guaino, G. Sheerin, D. Carty, T. McEnvoy, C. J. Barnes, V. Dhanak, and A. Santoni, Surf. Sci. **544**, 121 (2003).
[26]C. R. Parkinson, M. Walker, and C. F. McConville, Surf. Sci. **545**, 19 (2003).
[27]M. Walker, Ph.D. thesis, University of Warwick, 2006; see [http://www.caiciss.co.uk].
[28]J. F. van der Veen, Surf. Sci. Rep. **5**, 199 (1985).
[29]P. Bailey, T. C. Q. Noakes, and D. P. Woodruff, Surf. Sci. **426**, 358 (1999); also see [http://www.dl.ac.uk/MEIS].
[30]R. G. Musket, W. McLean, C. A. Colmenares, D. M. Makowiecki, and W. J. Siekhaus, Appl. Surf. Sci. **10**, 143 (1982).
[31]D. Brown, P. D. Quinn, D. P. Woodruff, T. C. Q. Noakes, and P. Bailey, Surf. Sci. **497**, 1 (2002).
[32]R. M. Tromp, M. Copel, M. C. Reuter, M. Horn Von Hoegen, J. Speidell, and R. Koudijs, Rev. Sci. Instrum. **62**, 2679 (1991).
[33]R. M. Tromp and J. F. van der Veen, Surf. Sci. **133**, 159 (1983).
[34]J. W. M. Frenken, J. F. van der Veen, and R. M. Tromp, Nucl. Instrum. Meth. B **17**, 334 (1986).
[35]H. Niehus, W. Heiland, and E. Taglauer, Surf. Sci. Rep. **17**, 213 (1993).
[36]T. C. Q. Noakes, P. Bailey, and D. P. Woodruff, Nucl. Instrum. Meth. B **136–138**, 1125 (1998).
[37]T. C. Q. Noakes, P. Bailey, C. F. McConville, C. R. Parkinson, M. Draxler, J. Smerdon, J. Ledieu, R. McGrath, A. R. Ross, and T. A. Lograsso, Surf. Sci. **583**, 139 (2005).
[38]T. J. Wood, C. Bonet, T. C. Q. Noakes, P. Bailey, and S. P. Tear, Surf. Sci. **598**, 120 (2005).
[39]T. E. Jones, T. C. Q. Noakes, P. Bailey, and C. J. Baddeley, Surf. Sci. **600**, 2129 (2006).
[40]H. Niehus and R. Spitzl, Surf. Interface Anal. **17**, 287 (1991).
[41]D. E. Fowler and J. V. Barth, Phys. Rev. B **52**, 2117 (1995).
[42]M. Walker, M. G. Brown, M. Draxler, L. Fishwick, M. G. Dowsett, and C. F. McConville, Surf. Sci. **605**, 107 (2011).
[43]P. Gilmore and C. T. Kelley, SIAM J. Optim. **5**, 269 (1995).
[44]T. D. Choi, O. J. Eslinger, C. T. Kelley, and J. W. D. M. Etheridge, Optimization and Engineering **1**, 9 (2000).
[45]R. Palangsuntikul, R. Polly, and B. Hartke, Phys. Chem. Chem. Phys. **6**, 5456 (2004).
[46]C. T. Kelley, *Iterative Methods for Optimization* (Society for Industrial and Applied Mathematics, Philadelphia, 1999).
[47]K. R. Fowler, J. P. Reese, C. E. Kees, J. E. Dennis Jr., C. T. Kelley, C. T. Miller, C. Audet, A. J. Booker, G. Couture, R. W. Darwin, M. W. Farthing, D. E. Finkel, J. M. Gablonsky, G. Gray, and T. G. Kolda, Adv. Water Resour. **31**, 743 (2008).
[48]L. S. Coelho and V. C. Mariani, Chaos, Solitons and Fractals **39**, 510 (2009).
[49]R. G. Carter, J. M. Gablonsky, A. Patrick, C. T. Kelley, and O. J. Eslinger, Optimization and Engineering **2**, 139 (2001).
[50]L. E. Davis, N. C. MacDonald, P. W. Palmberg, G. E. Riach, and R. E. Weber, *Handbook of Auger Electron Spectroscopy*, 2nd ed. (Physical Electronics Institute, Eden Prairie, 1976).